Slotless PM machines with skewed winding shapes

This article has been accepted for publication in a future issue of this journal, but has not been fully edited. Content may change prior to final publication. Citation information: DOI 10.1109/TMAG.2016.2586740, IEEE Transactions on Magnetics

Slotless PM machines with skewed winding shapes: 3D electromagnetic semi-analytical model

S. Jumayev[1], K.O. Boynov[1], J.J.H. Paulides[1], E.A. Lomonova[1], and J. Pyrhönen[2]

[1]Electrical Engineering Department, Eindhoven University of Technology, Eindhoven 5612 AZ, The Netherlands
[2]Electrical Engineering Department, Lappeenranta University of Technology, Lappeenranta 53850, Finland

The 3D modeling technique presented in this paper, predicts, with high accuracy, electromagnetic fields and corresponding dynamic effects in conducting regions for rotating machines with slotless windings, e.g. self-supporting windings. The presented modeling approach can be applied to a wide variety of slotless winding configurations, including skewing and/or different winding shapes. It is capable to account for induced eddy-currents in the conductive rotor parts, e.g. permanent magnet eddy-current losses, albeit not iron and winding AC losses. The specific focus of this paper is to provide the reader with the complete implementation and assumptions details of such a 3D semi-analytical approach, which allows model validations with relatively short calculation times. This model can be used to improve future design optimizations for machines with 3D slotless windings. It has been applied, in this paper, to calculate fixed parameter Faulhaber, Rhombic, and Diamond slotless PM machines to illustrate accuracy and applicability.

***Index Terms*—3D harmonic modeling, Fourier, BLDC PM machine, slotless winding, Faulhaber, rhombic, self-supporting winding, rotor eddy-current losses, high-speed.**

I. Introduction

SLOTLESS rotating permanent magnet (PM) machines are being employed in low to medium power industrial applications, such as medical, aerospace, factory automation, etc. Their 3D design evaluation would benefit from a fast electromagnetic modeling tool that does not suffer from long computational times when accuracy is paramount. Indeed, especially for design optimization procedures, computational time is even more important due to the required evaluation of a large field of design solutions. Thus analytical or semi-analytical modeling techniques are superior over numerical inasmuch as they usually require shorter computational times.

(Semi-)Analytical modeling of slotless AC machines is not a trivial task considering the fact that slotless windings have a large variety of configurations with complex geometries. Although in some configurations, e.g. toroidal, concentrated, distributed overlapping winding machines, the modeling can be reduced to a 2-dimensional (2D) problem due to the sole presence of an axial current component [1], [2], [3], [4]. However for some slotless winding machines, this 2D simplification is not applicable due the presence of skewing and/or different winding shapes, e.g. Faulhaber (also called helical and skewed), rhombic, and diamond winding, which are shown in Fig. 1. Here, the conductors can be skewed for half an electrical period, which implies both and axial and circumferential current component. This necessitates a 3-dimensional (3D) electromagnetic model to be implemented.

These 3D magnetic field modeling techniques have been reported in several papers. For example, the authors of [5] have presented the magnetic field modeling of a Faulhaber winding based on the numerical solution of the Biot-Savart law. In [6], [7] analytical models of magnetic field in machines with Faulhaber (helical) winding have been presented. The results obtained by these models are accurate, however do not consider induced rotor eddy-currents losses. These effects have been presented in [8], however the model contains an assumption which introduces an error in the rotor eddy-current

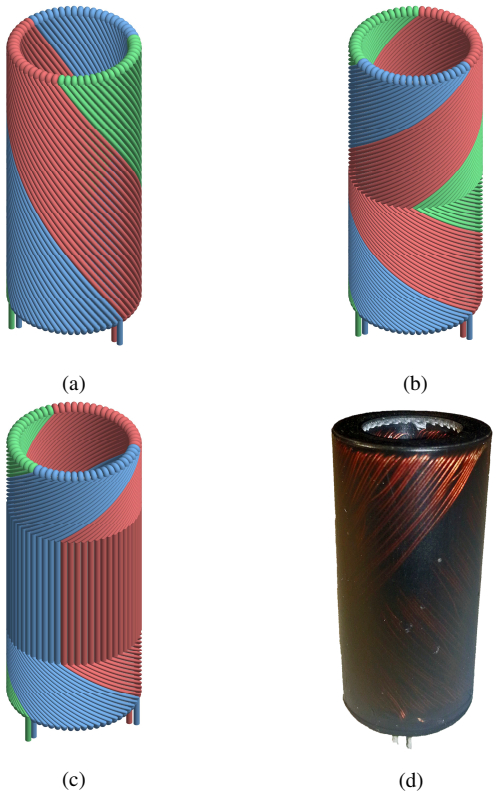

Figure 1: 3D representation of a 3-phase a) Faulhaber b) rhombic and c) diamond windings for rotating machines, d) photo of a potted 3-phase Faulhaber winding.

Corresponding author: S. Jumayev (e-mail: s.jumayev@tue.nl).

This article has been accepted for publication in a future issue of this journal, but has not been fully edited. Content may change prior to final publication. Citation information: DOI 10.1109/TMAG.2016.2586740, IEEE Transactions on Magnetics

calculations if rotor overhang is present. A possibility to overcome this assumption is to add air regions at the rotor sides (on front and rear) and implement a 3D mode-matching technique [9]. However, the model in this case is extremely complex to be derived and solved, which dramatically increases the calculation time.

In this paper a generalized and relatively fast 3D approach to model the armature reaction field of slotless winding PM machines is presented. The electromagnetic field calculation is based on the so-called Harmonic modeling which assumes the direct solution of the quasi-static Maxwell's equations. The winding space distribution is assessed through 2D Fourier series which conveniently describes the distribution of complex winding geometries. Moreover, 2D Fourier series allows to improve the accuracy of the modeling, for example compared to [8], by extending the axial boundaries of the winding distribution, which is difficult with 1D Fourier series. The 2D Fourier series contains 2D and 3D components simultaneously that forces to implement 2D or 3D Harmonic modeling for the same model, which is thoroughly explained in this paper. An additional feature of the presented approach is ability to account for the eddy-current losses and the eddy-current reaction field.

II. Harmonic Modeling in Cylindrical Coordinates

In order to derive a 3D Harmonic Model (HM) the following assumptions have been considered:

- The HM model is based on the quasi-static Maxwell's equations;
- Materials are isotropic (i.e. both relative permeability and conductivity remain the same in different directions);
- Soft-magnetic material parts (iron) are infinitely permeable;
- Winding current is modeled by linear current density, which assumes infinitely thin winding, placed on a boundary;
- The model is periodic in both axial and circumferential direction;
- Skin and proximity effects in conductors are not accounted for;
- Balanced 3-phase currents in the windings are considered;
- Back iron and rotor length are equal;
- The internal PM magnetization is zero.

In HM, the magnetic field is derived using the magnetic vector potential. Keeping in mind that the magnetic field is the solenoidal vector field ($\nabla \cdot \vec{B} = 0$), the magnetic vector potential is introduced as

$$\vec{B} = \nabla \times \vec{A}, \tag{1}$$

where $\vec{B}$ is the magnetic flux density [T] and $\vec{A}$ is the magnetic vector potential [Wb/m]. Combining the quasi-static Maxwell's equations and constitutive equations in electromagnetism, under the Coulomb gauge condition ($\nabla \cdot \vec{A} = 0$), results in

$$\nabla^2 \vec{A} = \mu_\mathrm{r}\mu_0\sigma\frac{\partial \vec{A}}{\partial t} - \mu_\mathrm{r}\mu_0\vec{J} - \nabla \times \vec{B}_\mathrm{rem}, \tag{2}$$

where μ_0 is the magnetic permeability of vacuum [H/m], μ_r the relative permeability of the material, σ the electric conductivity [S], $\vec{J}$ the current density [A/m^2], and $\vec{B}_\mathrm{rem}$ the remanent flux density of a material [T]. It should be stated that the rotor eddy-current component caused by the moving conducting rotor in the magnetic field is not present in this equation, but accounted for by considering the problem in the rotor reference frame which is introduced in Section III. Equation (2) is the so-called governing equation which relates the magnetic vector potential to the two magnetic field sources in PM machines, i.e. the excitation magnetic field originated from the PM as defined by $\vec{B}_\mathrm{rem}$, and the armature reaction field source as described by $\vec{J}$. This paper concentrates on calculating the armature reaction, hence the PM field can be omitted in the calculations as it does not generate any rotor eddy-currents in slotless PM machines. It is, however, relatively simple to assess the PM field using [1], [2], [3], [4], if needed. The current density in (2) can be represented as a linear current density on a boundary, and therefore is reduced to the Helmholtz equation

$$\nabla^2 \vec{A} = \mu_\mathrm{r}\mu_0\sigma\frac{\partial \vec{A}}{\partial t}. \tag{3}$$

This represents the governing equation in the conducting region that facilitates modeling of induced eddy-currents. For the air region where the conductivity $\sigma = 0$, the governing equation takes the form of Laplace equation

$$\nabla^2 \vec{A} = 0. \tag{4}$$

In general the HM assumes the division into regions with different electromagnetic properties, i.e. with different conductivity and permeability, where the field behavior in each region is governed by (3) or (4). Solutions of these governing equations are obtained by separation of variables. The solutions contain unknown coefficients which are determined by solving a system of equations based on the boundary information between considered regions, as discussed further.

A. 2D Harmonic modeling

In radial flux rotating machines electromagnetic torque is created by axial current components, thus if the model is limited to axial current components, only axial magnetic vector potentials have to be present. Therefore, a 2D HM can be used, where the magnetic flux density in a cylindrical (polar) coordinate system is expressed as

$$\vec{B} = \frac{1}{r}\frac{\partial A_\mathrm{z}}{\partial \theta}\vec{e}_\mathrm{r} - \frac{\partial A_\mathrm{z}}{\partial r}\vec{e}_\theta. \tag{5}$$

where $\vec{e}_\mathrm{r}$ and $\vec{e}_\theta$ are the unit vectors in the radial and circumferential (azimuthal) directions. The complete derivation of the 2D HM in cylindrical (polar) coordinates (r, θ) is thoroughly reported in [1], [2] and [4].

This article has been accepted for publication in a future issue of this journal, but has not been fully edited. Content may change prior to final publication. Citation information: DOI 10.1109/TMAG.2016.2586740, IEEE Transactions on Magnetics

1) Solution of the Laplace and Helmholtz equations

The complex form solution of (3) in cylindrical (polar) coordinate system with only axial component of the vector potential is given as

$$A_{\mathrm{z}}(\nu)=\begin{cases}(C(\nu)I_{\nu}(\beta r)+D(\nu)K_{\nu}(\beta r))\mathrm{e}^{\mathrm{j}(\nu\theta+\omega_{\mathrm{r}}t)}, & \text{if } \beta\neq 0\\ (C(\nu)r^{-\nu}+D(\nu)r^{\nu})\mathrm{e}^{\mathrm{j}(\nu\theta+\omega_{\mathrm{r}}t)}, & \text{if } \beta=0\end{cases}, \tag{6}$$

$$\beta^2=\mathrm{j}\mu_{\mathrm{r}}\mu_0\sigma\omega_{\mathrm{r}},$$

where I and K are the modified Bessel functions of the first and second kind, C and D the unknown coefficients, ν the space harmonic order, j the imaginary unit, and ω_{r} the relative angular velocity between the media and magnetic field. The solution of the Laplace equation (4) in complex form is written as

$$A_{\mathrm{z}}(\nu)=(C(\nu)r^{-\nu}+D(\nu)r^{\nu})\mathrm{e}^{\mathrm{j}(\nu\theta+\omega_{\mathrm{r}}t)}. \tag{7}$$

2) Boundary conditions

The boundary conditions between two regions are used to calculate the unknown coefficients of the solutions of Laplace (7) and Helmholtz (6) equations, expressed as

$$\vec{n}\cdot(\vec{B}_1-\vec{B}_2)=0, \tag{8}$$

$$\vec{n}\times(\vec{H}_1-\vec{H}_2)=\vec{K}, \tag{9}$$

where subscript 1 and 2 indicate variable of the first and second interfacing regions, $\vec{K}$ the linear current density [A/m], $\vec{n}$ the surface normal, and $\vec{H}$ the magnetic field strength [A/m]. The latter can be determined by the following relation

$$\vec{H}=\frac{\vec{B}}{\mu_{\mathrm{r}}\mu_0}. \tag{10}$$

B. 3D Harmonic modeling

If the equivalent linear current density is not limited to the axial current components, as e.g. in Faulhaber, rhombic and etc. windings, also circumferential current components are present. Thus two components of the magnetic vector potential have to be introduced which necessitates a 3D HM implementation. Unfortunately, in cylindrical coordinates the solutions of (3) and (4) cannot be determined by the magnetic vector potential [10]. However, the solution of these equations can be obtained by introducing a second order vector potential. Keeping in mind $\nabla\cdot\vec{A}=0$, this second order magnetic vector potential, $\vec{W}$, is introduced as [11]

$$\vec{A}=\nabla\times\vec{W}. \tag{11}$$

$\vec{W}$ consists of two orthogonal scalar potentials, W_1 and W_2 and in cylindrical coordinates is given by [12]

$$\vec{W}=W_1\vec{e}_{\mathrm{z}}+\nabla\times W_2\vec{e}_{\mathrm{z}}, \tag{12}$$

where W_1 and W_2 are the magnetic scalar potential functions [Wb] and [Wbm], respectively, and $\vec{e}_{\mathrm{z}}$ the unit vector in axial direction. Substituting (12) into (3), separate expressions for W_1 and W_2 are

$$\begin{aligned}\nabla^2W_1&=\beta^2W_1,\\ \nabla^2W_2&=\beta^2W_2,\\ \beta^2&=\mathrm{j}\mu_{\mathrm{r}}\mu_0\sigma\omega_{\mathrm{r}}.\end{aligned} \tag{13}$$

These equations are the governing equations in the conducting region of the 3D HM. Using (11), (12) and (13) the magnetic vector potential is expressed as

$$\vec{A}=(\frac{1}{r}\frac{\partial W_1}{\partial\theta}+\frac{\partial^2W_2}{\partial r\partial z})\vec{e}_{\mathrm{r}}+(\frac{1}{r}\frac{\partial^2W_2}{\partial\theta\partial z}-\frac{W_1}{\partial r})\vec{e}_{\theta}+ +(\frac{\partial^2W_2}{\partial z^2}-\beta^2W_2)\vec{e}_{\mathrm{z}}. \tag{14}$$

The expression for the vector potential is substituted into (1), and the magnetic flux density inside the conducting region is given as

$$\vec{B}=(\frac{\partial^2W_1}{\partial r\partial z}-\frac{\beta^2}{r}\frac{\partial W_2}{\partial\theta})\vec{e}_{\mathrm{r}}+(\frac{1}{r}\frac{\partial^2W_1}{\partial\theta\partial z}+\beta^2\frac{W_2}{\partial r})\vec{e}_{\theta}+ +(\frac{\partial^2W_1}{\partial z^2}-\beta^2W_1)\vec{e}_{\mathrm{z}}. \tag{15}$$

The governing equation for the air region is obtained by simply setting β to zero. Then from (15) it can be observed that when β is zero the scalar potential W_2 does not contribute to the flux density. Therefore, using (13) the governing equation for the air region is

$$\nabla^2W_1=0. \tag{16}$$

The expression for the flux density in the air region is given by

$$\vec{B}=\frac{\partial^2W_1}{\partial r\partial z}\vec{e}_{\mathrm{r}}+\frac{1}{r}\frac{\partial^2W_1}{\partial\theta\partial z}\vec{e}_{\theta}+\frac{\partial^2W_1}{\partial z^2}\vec{e}_{\mathrm{z}}. \tag{17}$$

1) Solution of the Laplace and Helmholtz equations

The solution of (13) is also determined by separation of variables which results in [9]

$$\begin{aligned}W_1(\nu,\omega_{\mathrm{z}})&=(C_1(\nu,\omega_{\mathrm{z}})I_{\nu}(\xi r)+D_1(\nu,\omega_{\mathrm{z}})K_{\nu}(\xi r))\cdot\\ &\quad\cdot(F_1(\nu,\omega_{\mathrm{z}})\cos(\omega_{\mathrm{z}}z)+G_1(\nu,\omega_{\mathrm{z}})\sin(\omega_{\mathrm{z}}z))\mathrm{e}^{\mathrm{j}(\nu\theta+\omega_{\mathrm{r}}t)},\\ W_2(\nu,\omega_{\mathrm{z}})&=(C_2(\nu,\omega_{\mathrm{z}})I_{\nu}(\xi r)+D_2(\nu,\omega_{\mathrm{z}})K_{\nu}(\xi r))\cdot\\ &\quad\cdot(F_2(\nu,\omega_{\mathrm{z}})\cos(\omega_{\mathrm{z}}z)+G_2(\nu,\omega_{\mathrm{z}})\sin(\omega_{\mathrm{z}}z))\mathrm{e}^{\mathrm{j}(\nu\theta+\omega_{\mathrm{r}}t)},\\ \xi^2&=\omega_{\mathrm{z}}^2+\beta^2,\end{aligned} \tag{18}$$

where C, D, F, G are unknown constants calculated using boundary conditions, and ω_z is the spatial frequency in the z-direction. For the Laplace equation (16) the solution takes the form [9]

This article has been accepted for publication in a future issue of this journal, but has not been fully edited. Content may change prior to final publication. Citation information: DOI 10.1109/TMAG.2016.2586740, IEEE Transactions on Magnetics

$$W_1(\nu,\omega_z) = (C(\nu,\omega_z)I_\nu(\omega_z r) + D(\nu,\omega_z)K_\nu(\omega_z r))\cdot \\ \cdot (F(\nu,\omega_z)\cos(\omega_z z) + G(\nu,\omega_z)\sin(\omega_z z))\mathrm{e}^{\mathrm{j}(\nu\theta+\omega_t t)}. \tag{19}$$

2) Boundary conditions

The boundary conditions for 3D HM include (8), (9) and the boundary information of the electric field strength, expressed as

$$\vec{n}\times(\vec{E}_1 - \vec{E}_2) = 0, \tag{20}$$

where $\vec{E}$ is electric field strength [V/m], which can be calculated using

$$\vec{E} = -\frac{\partial \vec{A}}{\partial t}. \tag{21}$$

It needs noting that only one component of electrical field (axial or tangential) requires a boundary condition (20). For example, constraining the axial electrical field strength omits the use of the circumferential one.

C. Rotor eddy-current losses

As the rotor PM field is neglected, the power transfered to torque production is zero. However, the armature reaction causes rotor eddy-current losses, which can be calculated by integrating the Poynting vector over the rotor surface. For radial flux rotating machines, where the radial component of the vector potential is zero, the rotor eddy-current losses are calculated as

$$P = -\frac{1}{2}\oint_{S_{\text{rotor}}} \mathrm{Re}(E_z H_\theta^* - E_\theta H_z^*)\mathrm{d}S_{\text{rotor}}, \tag{22}$$

where $\vec{H}^*$ is the conjugated magnetic field strength [A/m] and S_{rotor} the rotor surface [m^2].

III. Distribution of Linear Current Density

Modeling winding regions with imposed currents in cylindrical coordinates does not seem possible by means of first and second order vector potentials [13]. Thus the winding is modeled as an air region and linear current density, imposed on the iron bore surface. If this linear current density is solely distributed along the axial direction, a 2D HM can be used, e.g. for machines with toroidal or concentrated slotless windings. However, if an axial and circumferential components are present (see Fig. 2), the linear current density can be written as

$$\vec{K} = K_z\vec{e}_z + K_\theta\vec{e}_\theta, \tag{23}$$

where K_z and K_θ are the axial and circumferential linear current density components, respectively, [A/m].

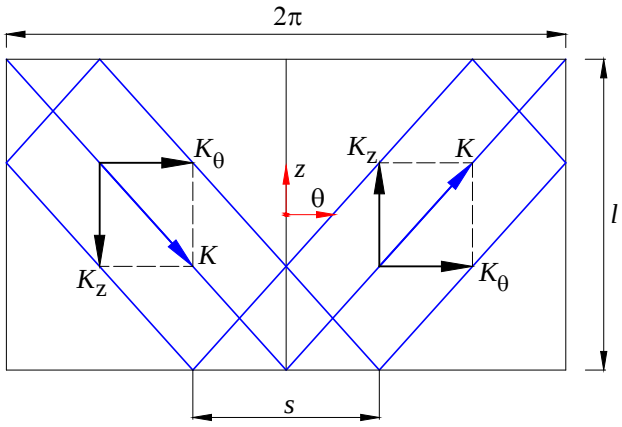

Figure 2: A phase coil contour of a Faulhaber winding. The blue arrows indicate the linear current density, and black arrows the axial and circumferential components, correspondingly.

A. Axial component of linear current density

The axial component of the linear current density in a single phase can be written as

$$K_z(\theta,z,t) = \frac{Ni(t)}{sr} f_z(\theta,z), \tag{24}$$

where N is the phase turn number, i the instantaneous value of phase current [A], r the radius at which the linear current density is defined [m], s the phase spread in circumference [rad], t time [s], and $f_z(\theta,z)$ the distribution function dependent on the geometry of the winding. This distribution function can be generally approximated through 2D Fourier series as

$$\begin{aligned} f_{z,\text{approx}}(\theta,z) = \sum_{\substack{\nu=0\\ m=0}}^{\infty} \big[& c_{ss}(\nu,m)\sin(\omega_\theta\theta)\sin(\omega_z z) + \\ & + c_{sc}(\nu,m)\sin(\omega_\theta\theta)\cos(\omega_z z) + \\ & + c_{cs}(\nu,m)\cos(\omega_\theta\theta)\sin(\omega_z z) + \\ & + c_{cc}(\nu,m)\cos(\omega_\theta\theta)\cos(\omega_z z)\big], \\ \omega_\theta = \frac{\nu 2\pi}{T_\theta}, & \\ \omega_z = \frac{m 2\pi}{T_z}, & \end{aligned} \tag{25}$$

where ω_θ and ω_z are the spacial frequencies in the θ- and z-direction, and T_θ and T_z the periodicities in the θ- and z-direction. The coefficients c_{ss}, c_{sc}, c_{cs} and c_{cc} are derived by the following integrals

This article has been accepted for publication in a future issue of this journal, but has not been fully edited. Content may change prior to final publication. Citation information: DOI 10.1109/TMAG.2016.2586740, IEEE Transactions on Magnetics

$$
\begin{aligned}
c_{\mathrm{ss}}(\nu,m) &= \frac{\kappa}{4T_\theta T_\mathrm{z}} \int_0^{T_\mathrm{z}} \int_0^{T_\theta} f_\mathrm{z}(\theta,z) \sin(\omega_\theta \theta) \sin(\omega_\mathrm{z} z)\, d\theta dz,\\
c_{\mathrm{sc}}(\nu,m) &= \frac{\kappa}{4T_\theta T_\mathrm{z}} \int_0^{T_\mathrm{z}} \int_0^{T_\theta} f_\mathrm{z}(\theta,z) \sin(\omega_\theta \theta) \cos(\omega_\mathrm{z} z)\, d\theta dz,\\
c_{\mathrm{cs}}(\nu,m) &= \frac{\kappa}{4T_\theta T_\mathrm{z}} \int_0^{T_\mathrm{z}} \int_0^{T_\theta} f_\mathrm{z}(\theta,z) \cos(\omega_\theta \theta) \sin(\omega_\mathrm{z} z)\, d\theta dz,\\
c_{\mathrm{cc}}(\nu,m) &= \frac{\kappa}{4T_\theta T_\mathrm{z}} \int_0^{T_\mathrm{z}} \int_0^{T_\theta} f_\mathrm{z}(\theta,z) \cos(\omega_\theta \theta) \cos(\omega_\mathrm{z} z)\, d\theta dz,
\end{aligned}
\tag{26}
$$

where

$$
\kappa = \begin{cases} 4, & \text{for } \nu > 0,\ m > 0 \\ 2, & \text{for } \nu = 0,\ m > 0 \\ 2, & \text{for } \nu > 0,\ m = 0 \\ 1, & \text{for } \nu = 0,\ m = 0 \end{cases}. \tag{27}
$$

The integral limits in (26) can be set by linear equations to describe winding skewing [14]. The practical implementation of the 2D Fourier series is given in the Appendices.

For three phase rotating machines the phase coils are mutually shifted by $2\pi/3$, hence the phase currents are given as

$$
\begin{aligned}
i(t) &= \sum_{k=1}^{\infty} \hat{I}(k) \cos(k(\omega t + x)), \\
x &= \left(0, \frac{2\pi}{3}, \frac{4\pi}{3}\right),
\end{aligned}
\tag{28}
$$

where $\hat{I}$ is the current amplitude of each time harmonic order [A], k the time harmonic order and ω the angular frequency [rad/s]. Substituting (25) and (28) into (24) results in a Fourier series representation of the axial linear current density

$$
\begin{aligned}
K_\mathrm{z}(\theta,z,t) = \sum_{\substack{m=0 \\ k=1 \\ L=-\infty}}^{\infty} & \big[\hat{K}_{\mathrm{ss}}(m,k,L) \sin((3L-k)\theta + k\omega t) \sin(\omega_\mathrm{z} z) + \\
& + \hat{K}_{\mathrm{sc}}(m,k,L) \sin((3L-k)\theta + k\omega t) \cos(\omega_\mathrm{z} z) + \\
& + \hat{K}_{\mathrm{cs}}(m,k,L) \cos((3L-k)\theta + k\omega t) \sin(\omega_\mathrm{z} z) + \\
& + \hat{K}_{\mathrm{cc}}(m,k,L) \cos((3L-k)\theta + k\omega t) \cos(\omega_\mathrm{z} z)\big],
\end{aligned}
\tag{29}
$$

where L is an integer number and $\hat{K}$ the amplitude of Fourier series components.

Since the solutions of the governing equations (6), (7), (18), and (19) are in the complex form, the linear current density expression (29), for the simplicity reasons, is transformed to the complex form as

$$
\begin{aligned}
K_\mathrm{z}(\theta,z,t) = \sum_{\substack{m=0 \\ k=1 \\ L=-\infty}}^{\infty} & \big[\hat{K}_{\mathrm{ss}}(m,k,L) \mathrm{e}^{\mathrm{j}((3L-k)\theta + k\omega t)} \sin(\omega_\mathrm{z} z) + \\
& + \hat{K}_{\mathrm{sc}}(m,k,L) \mathrm{e}^{\mathrm{j}((3L-k)\theta + k\omega t)} \cos(\omega_\mathrm{z} z) + \\
& + \hat{K}_{\mathrm{cs}}(m,k,L) \mathrm{e}^{\mathrm{j}((3L-k)\theta + k\omega t)} \sin(\omega_\mathrm{z} z) + \\
& + \hat{K}_{\mathrm{cc}}(m,k,L) \mathrm{e}^{\mathrm{j}((3L-k)\theta + k\omega t)} \cos(\omega_\mathrm{z} z)\big].
\end{aligned}
\tag{30}
$$

This complex linear current density can be transformed from the complex domain back to (29), by taking the real or imaginary part of each component.

B. Circumferential component of linear current density

The circumferential component of the linear current density can be derived using the same procedure, alternatively from the continuity equation as

$$
\frac{\partial K_\mathrm{z}}{\partial z} = -\frac{1}{r} \frac{\partial K_\theta}{\partial \theta}. \tag{31}
$$

However, there is no need for the circumferential component of the linear current density for the field calculation. This statement results from the continuity equation with absence of the free charge conservation and Ampere's law. If on the boundary with linear current density the transition conditions for the normal and a single tangential (axial or circumferential) magnetic field components have been satisfied, the second tangential component is also satisfied [12].

C. Linear current density in rotor reference frame

The axial component of the linear current density, (30), is given in the stator reference frame. This means that the harmonics are traveling with respect to the stator. However for the rotor eddy-current calculation the expression should be transferred to the rotor reference frame, since only the harmonics rotating with respect to the rotor induce eddy-currents. Therefore, the angular position of the rotor is linked to the angular position of the stator through the angular velocity of the rotor as

$$
\theta = \theta_\mathrm{r} + \omega t, \tag{32}
$$

where θ_r is the angular position in the rotor reference frame [rad]. Substituting (32) equation into (30) results in the expression of the axial component of the linear current density in the rotor reference frame

This article has been accepted for publication in a future issue of this journal, but has not been fully edited. Content may change prior to final publication. Citation information: DOI 10.1109/TMAG.2016.2586740, IEEE Transactions on Magnetics

$$K_{\mathrm{z}}(\theta_{\mathrm{r}},z,t)=\sum_{\substack{m=0\\k=1\\L=-\infty}}^{\infty}\Big[\hat{K}_{\mathrm{ss}}(m,k,L)\mathrm{e}^{\mathrm{j}((3L-k)\theta_{\mathrm{r}}+3L\omega t)}\sin(\omega_{\mathrm{z}}z)+ +\hat{K}_{\mathrm{sc}}(m,k,L)\mathrm{e}^{\mathrm{j}((3L-k)\theta_{\mathrm{r}}+3L\omega t)}\cos(\omega_{\mathrm{z}}z)+ +\hat{K}_{\mathrm{cs}}(m,k,L)\mathrm{e}^{\mathrm{j}((3L-k)\theta_{\mathrm{r}}+3L\omega t)}\sin(\omega_{\mathrm{z}}z)+ +\hat{K}_{\mathrm{cc}}(m,k,L)\mathrm{e}^{\mathrm{j}((3L-k)\theta_{\mathrm{r}}+3L\omega t)}\cos(\omega_{\mathrm{z}}z)\Big]. \tag{33}$$

IV. Three-Dimensional Model Synthesis of Slotless Winding Machines

This section describes the realization procedure of the 3D HM. For validation, the model is implemented for fixed parameter Faulhaber, rhombic and diamond shaped windings, as shown in Fig. 3. The axial component of the linear current density of these windings is given in section Appendix.

Only the 3D HM synthesis for a PM machine with rhombic winding is derived in detail in this paper, i.e. on the slotless PM machine as shown in Fig. 4a. Here, the rotor is completely made of a diametrically magnetized single PM, and, as discussed before, the PM excitation field is not considered, thus the PM is modeled as a conducting region. The back iron is infinitely permeable, and the winding is represented by an air region with linear current density on its boundary (between air and back-iron). The resultant model consists of two regions: the PM and air gap, as shown in Fig. 4b.

Finally, an important model detail is the axial periodicity. In [8], where the 3D HM of the Faulhaber winding machines is presented, the model has an axial periodicity of a single winding length. However, the rotor usually overhangs the winding, which influences the induced eddy-currents distribution, thus the assumption in [8] leads to an error in the rotor eddy-current estimation and magnetic field. To overcome this, the axial periodicity of the model is set to $T_{\mathrm{z}}=2l$ as shown in Fig. 4b. However, this axial periodicity automatically assumes that the back-iron length equals the axial periodicity. The authors realize that this is not a completely correct implementation, since ideally the axial periodicity should be equal to the rotor length. Nevertheless, this assumption simplifies the derivation of the linear current density expression and the obtained results are more accurate than the results shown in [8].

A. HM model of PM machine with rhombic winding

The implementation of the 3D HM starts with the derivation of the linear current density, which is, for the rhombic winding, given as

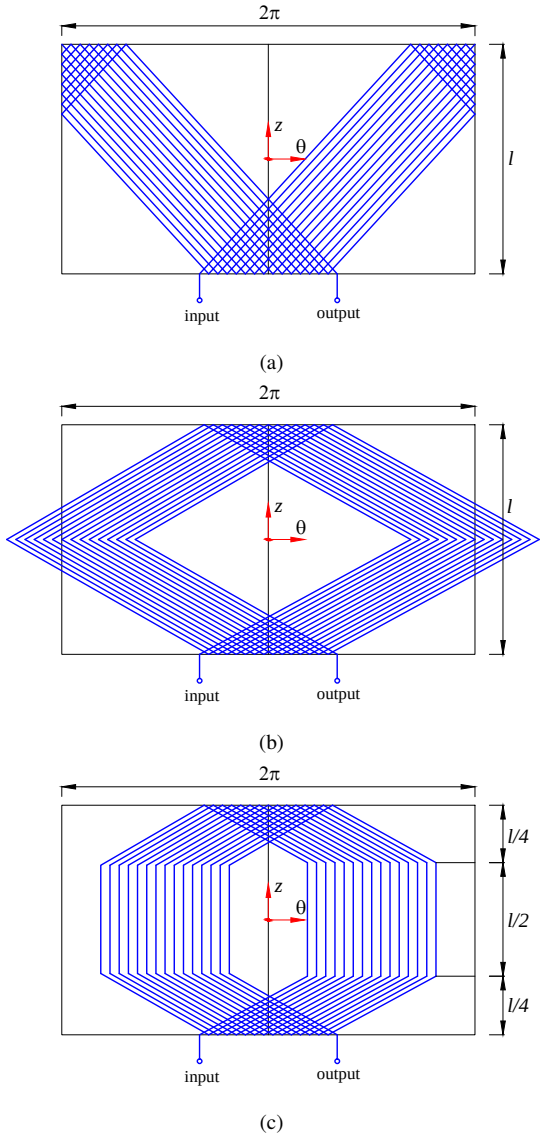

Figure 3: One phase coil of a) Faulhaber (helical), b) rhombic, and c) diamond slotless winding types.

$$K_{\mathrm{z}}(\theta_{\mathrm{r}},z,t)=K_{\mathrm{z1}}+K_{\mathrm{z2}}, \tag{34}$$

$$K_{\mathrm{z1}}=\sum_{\substack{m=1\\k=1\\L=-\infty}}^{\infty}\big(\hat{K}_{\mathrm{sc1}}(m,k,L)\cos(\omega_{\mathrm{z1}}z)\cdot \cdot\mathrm{e}^{\mathrm{j}((3L-k)\theta_{\mathrm{r}}+3L\omega t)},$$

$$K_{\mathrm{z2}}=\sum_{\substack{m=1\\k=1\\L=-\infty}}^{\infty}\big(\hat{K}_{\mathrm{sc2}}(m,k,L)\cos(\omega_{\mathrm{z2}}z)\cdot \cdot\mathrm{e}^{\mathrm{j}((3L-k)\theta_{\mathrm{r}}+3L\omega t)},$$

$$\omega_{\mathrm{z1}}=\frac{\left(3L-k-\frac{m}{2}\right)\pi}{l},$$

$$\omega_{\mathrm{z2}}=\frac{\left(3L-k+\frac{m}{2}\right)\pi}{l},$$

This article has been accepted for publication in a future issue of this journal, but has not been fully edited. Content may change prior to final publication. Citation information: DOI 10.1109/TMAG.2016.2586740, IEEE Transactions on Magnetics

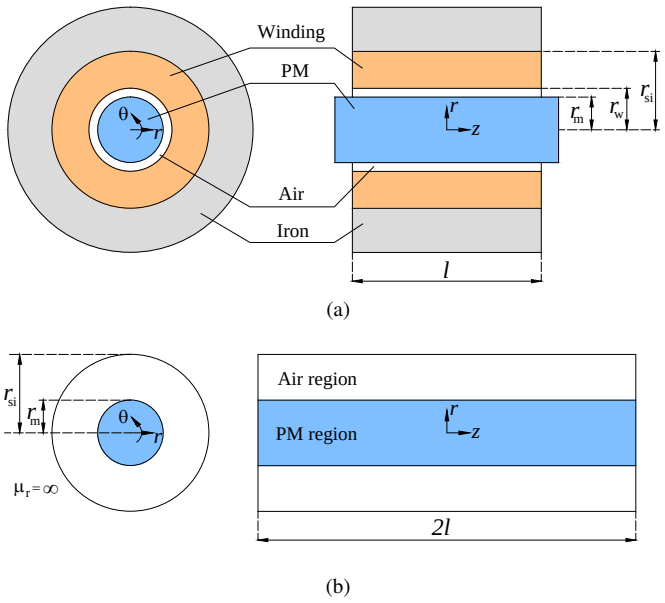

Figure 4: a) Cross-sections of a slotless PM machine with a shaftless rotor, b) Representation of the regions in the analytical model (iron is assumed to be infinitely permeable).

where $\hat{K}_{\text{sc1}}$ and $\hat{K}_{\text{sc2}}$ are linear current density component amplitudes [A/m]. These amplitude expressions are given in Appendix A, as well as the derivation of linear current density for the rhombic winding. Equation (34) contains two components, thus the superposition principle is used to obtain the field solution.

1) 3D harmonic model

Electromagnetic field behavior in the air region is described by the Laplace equation (16) and in the conducting region by the Helmholtz equation (13). The solution of these equations needs to comply with the linear current density distribution. Thus the magnetic scalar potentials (18) in the PM region should also consist of two components as the expression of the linear current density, where the first component can be written as

$$\begin{aligned}
W_{\text{1PM1}}(m,k,L) &= \sum_{\substack{m=1\\k=1\\L=-\infty}}^{\infty} C_{\text{1PM1}}(m,k,L) I_{3L-k}(\xi_{\text{PM1}} r)\cdot \\
&\quad \cdot \sin(\omega_{\text{z1}} z) \mathrm{e}^{\mathrm{j}((3L-k)\theta_{\text{r}}+3L\omega t)}, \\
W_{\text{2PM1}}(m,k,L) &= \sum_{\substack{m=1\\k=1\\L=-\infty}}^{\infty} C_{\text{2PM1}}(m,k,L) I_{3L-k}(\xi_{\text{PM1}} r)\cdot \\
&\quad \cdot \cos(\omega_{\text{z1}} z) \mathrm{e}^{\mathrm{j}((3L-k)\theta_{\text{r}}+3L\omega t)}, \qquad (35)\\
\beta^2_{\text{PM}} &= \mathrm{j}3L\omega\sigma_{\text{PM}}\mu_{\text{PM}}, \\
\xi^2_{\text{PM1}} &= \omega^2_{\text{z1}} + \beta^2_{\text{PM}},
\end{aligned}$$

and the second component as

$$\begin{aligned}
W_{\text{1PM2}}(m,k,L) &= \sum_{\substack{m=1\\k=1\\L=-\infty}}^{\infty} C_{\text{1PM2}}(m,k,L) I_{3L-k}(\xi_{\text{PM2}} r)\cdot \\
&\quad \cdot \sin(\omega_{\text{z2}} z) \mathrm{e}^{\mathrm{j}((3L-k)\theta_{\text{r}}+3L\omega t)}, \\
W_{\text{2PM2}}(m,k,L) &= \sum_{\substack{m=1\\k=1\\L=-\infty}}^{\infty} C_{\text{2PM2}}(m,k,L) I_{3L-k}(\xi_{\text{PM2}} r)\cdot \\
&\quad \cdot \cos(\omega_{\text{z2}} z) \mathrm{e}^{\mathrm{j}((3L-k)\theta_{\text{r}}+3L\omega t)}, \qquad (36)\\
\beta^2_{\text{PM}} &= \mathrm{j}3L\omega\sigma_{\text{PM}}\mu_{\text{PM}}, \\
\xi^2_{\text{PM2}} &= \omega^2_{\text{z2}} + \beta^2_{\text{PM}}.
\end{aligned}$$

Since the PM region inner radius is zero, the component that consists the modified Bessel function of the second kind is also zero. The solution of the Laplace equation also has two components, where the first component is

$$\begin{aligned}
W_{\text{a1}}(m,k,L) = \sum_{\substack{m=1\\k=1\\L=-\infty}}^{\infty} &(C_{\text{a1}}(m,k,L) I_{3L-k}(\omega_{\text{z1}} r) + \\
&+ D_{\text{a1}}(m,k,L) K_{3L-k}(\omega_{\text{z1}} r)) \sin(\omega_{\text{z1}} z) e^{\mathrm{j}((3L-k)\theta_{\text{r}}+3L\omega t)}, \qquad (37)
\end{aligned}$$

and the second component

$$\begin{aligned}
W_{\text{a2}}(m,k,L) = \sum_{\substack{m=1\\k=1\\L=-\infty}}^{\infty} &(C_{\text{a2}}(m,k,L) I_{3L-k}(\omega_{\text{z2}} r) + \\
&+ D_{\text{a2}}(m,k,L) K_{3L-k}(\omega_{\text{z2}} r)) \sin(\omega_{\text{z2}} z) \mathrm{e}^{\mathrm{j}((3L-k)\theta_{\text{r}}+3L\omega t)}. \qquad (38)
\end{aligned}$$

2) 2D harmonic model

A 2D HM is employed when the linear current density becomes z-independent, e.g. the current distribution is inherently independent of z, as one of the components of the diamond winding linear current density (see Appendix C), or when $\omega_{\text{z}} = 0$.

Similarly to the 3D model and taking (6) and (34), the solution in the PM region is

$$\begin{aligned}
A_{\text{z}}(k,L) = \sum_{\substack{k=1\\L=-\infty}}^{\infty} &\begin{cases} C_{\text{PM}}(k,L) I_{3L-k}(\beta_{\text{PM}} r)\cdot \\ \cdot \mathrm{e}^{\mathrm{j}((3L-k)\theta_{\text{r}}+3L\omega t)} & \text{if } L \neq 0, \\ C_{\text{PM}}(k,L) r^{\text{abs}(3L-k)}. \\ \cdot \mathrm{e}^{\mathrm{j}((3L-k)\theta_{\text{r}}+3L\omega t)} & \text{if } L = 0, \end{cases} \qquad (39)\\
\beta^2_{\text{PM}} &= \mathrm{j}\omega_{\text{r}}\mu_{\text{PM}}\sigma_{\text{PM}} = \mathrm{j}3L\omega\mu_{\text{PM}}\sigma_{\text{PM}}.
\end{aligned}$$

This solution contains both the first and second component of the linear current density distribution. For the air region the solution is

This article has been accepted for publication in a future issue of this journal, but has not been fully edited. Content may change prior to final publication. Citation information: DOI 10.1109/TMAG.2016.2586740, IEEE Transactions on Magnetics

$$A_z(k,L) = \sum_{\substack{k=1 \\ L=-\infty}}^{\infty} (C_a(k,L)r^{-(3L-k)} + D_a(k,L)r^{3L-k}) \cdot \cdot e^{j((3L-k)\theta_r + 3L\omega t)}. \quad (40)$$

3) Determination of unknown coefficients

To determine the unknown coefficients in (35)-(40), a system of equations based on the boundary condition information is composed, for the 3D HM as

$$\begin{cases} B_{rPM} - B_{ra} = 0, & \text{for } r = r_m \\ H_{\theta PM} - H_{\theta a} = 0, & \text{for } r = r_m \\ H_{zPM} - H_{za} = 0, & \text{for } r = r_m \\ H_{\theta a} = K_z, & \text{for } r = r_{si} \end{cases} \quad (41)$$

This system of equations consists of four equation which equals to the number of unknowns in the PM and air regions in the 3D HM. The system of equations for the 2D HM is

$$\begin{cases} B_{rPM} - B_{ra} = 0, & \text{for } r = r_m \\ H_{\theta PM} - H_{\theta a} = 0, & \text{for } r = r_m \\ H_{\theta a} = K_z, & \text{for } r = r_{si} \end{cases} \quad (42)$$

Consequently solving these system of equations for both components of the axial linear current density, the unknown coefficients calculated.

B. Calculation of rotor eddy-current losses

Equation (22) is used to calculate the rotor losses due to the induced eddy-currents, however analytically this equation is difficult to implement. This difficulty is related to the fact that magnetic and electric field strengths in (22) can have several components due to the linear current density distribution, which makes the analytical solution of the loss calculation rather complicated.

Therefore, a numerical approach is implemented that assumes the division of the rotor surface into small areas/elements (S_e), as shown in Fig. 5. The rotor eddy-current losses are calculated for each element separately and eventually summarized together. The values of the electrical and magnetic field strengths are determined in the center of these elements. Mathematically for the case of rhombic winding this can be formulated as

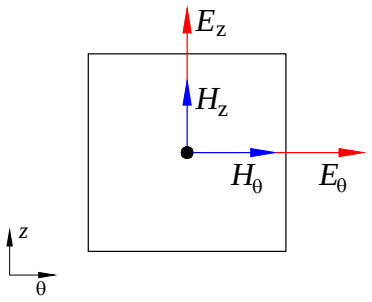

Figure 5: A sample of the area/element (S_e).

$$P = -\sum_{k=1}^{\infty}\sum_{v=1}^{V}\sum_{w=1}^{W} \frac{S_e}{2} \mathrm{Re}(E_z^{v,w}(k) H_\theta^{*v,w}(k) - E_\theta^{v,w}(k) H_z^{*v,w}(k)), \quad (43)$$

$$S_e = \frac{2\pi r_m T_z}{VW},$$

$$E^{v,w}(k) = \sum_{\substack{m=1 \\ L=-\infty}}^{\infty} (E_1^{v,w}(m,k,L) + E_2^{v,w}(m,k,L)),$$

$$H^{v,w}(k) = \sum_{\substack{m=1 \\ L=-\infty}}^{\infty} (H_1^{v,w}(m,k,L) + H_2^{v,w}(m,k,L)),$$

where v and w indicate the element position in z and θ directions, 1 and 2 are indexes corresponding to the quantities resulting from the first and second component of the rhombic winding linear current density, and V and W are number of elements in z and θ directions, thus $V \cdot W$ results in the number of elements the rotor is divided into.

V. Model Validation

The 3D semi-analytical model validation is done by comparison of radial flux densities and rotor eddy-current losses, obtained by the semi-analytical and 3D FEM models. The material and geometrical properties of the benchmark machines are summarized in Table I.

The software used to build the 3D FEM models is Flux 12 from Cedrat. The iron core permeability in the 3D FEM model is set to infinity, and the iron (axial) length is equal to the winding length l. The windings in FEM models are modeled by means of non-meshed coils which represent non-conducting conductor volumes with imposed current density.

Table I: Material and geometrical properties of the benchmark PM machines

Parameter [symbol]	Value
Speed [n]	10^5 rpm
Relative magnetic permeability of PM [μ_{rPM}]	1.05
Electric conductivity of PM [σ_{PM}]	5.9 10^5 S/m
Number of turns per coil [N]	16
Winding spread [s]	$2\pi/3$ rad
Machine active length [l]	20 mm
Magnet radius [r_m]	2.75 mm
Stator bore inner radius [r_{si}]	5 mm
Stator bore outer radius [r_{so}]	8 mm
Air-gap length [δ]	0.5 mm
L	-11÷11
m	1÷21
V, W	100

A. Magnetic flux density

The magnetic flux density radial components of the benchmark PM machines obtained by the semi-analytical model are illustrated in Fig. 6. These are extracted for the first time harmonic component with a phase current peak value of 1A. Figure 7 shows the relative difference of the radial magnetic flux densities obtained by the analytical model and the 3D FEM for the benchmark machines. The small

This article has been accepted for publication in a future issue of this journal, but has not been fully edited. Content may change prior to final publication. Citation information: DOI 10.1109/TMAG.2016.2586740, IEEE Transactions on Magnetics

difference indicates a good agreement between these models, where the maximum relative difference is less than 10% and the weighted mean value over the active part of the rotor is about 3%, respectively. Further, it can be seen that the difference replicates the winding geometries. Additionally, to give a visual impression of the magnetic flux density difference between the semi-analytical and 3D FEM models, where 2D plots of radial flux densities of the benchmark machines are illustrated in Fig. 8.

B. Rotor eddy-current losses

To summarize the results of the rotor eddy-current loss calculation, Table II provides the losses per harmonic for the rotating speed of 100 000 rpm with both the semi-analytical and FEM analysis, respectively. Within this simulation, the phase current amplitude for all time harmonic components for the convenience is assumed to be 1A. This, however, represents a theoretical value, since it is important to account for the rotor eddy-current losses in PM machines, especially in high-speed ones, to avoid thermal overloading of the rotor. This summary illustrates that the difference between the results of the semi-analytical and FEM analysis does not exceed 5%, which validates the 3D semi-analytical model. It needs noting that this model does allow the eddy-current loss calculation for all integer time harmonics, however without triplet harmonics due to the considered three phase system.

Table II: Rotor eddy-current losses versus the time harmonic order (semi-analytical - SANA, 3D FEM - FEM)

P [W] \ k	1	7	13	23	35
Faulhaber					
SANA	$3.1{\cdot}10^{-5}$	$9.5{\cdot}10^{-3}$	$3.7{\cdot}10^{-2}$	0.139	0.288
FEM	$3.0{\cdot}10^{-5}$	$9.5{\cdot}10^{-3}$	$3.6{\cdot}10^{-2}$	0.132	0.289
Rhombic					
SANA	$1.6{\cdot}10^{-5}$	$8.2{\cdot}10^{-3}$	$3.2{\cdot}10^{-2}$	0.121	0.245
FEM	$1.7{\cdot}10^{-5}$	$8.3{\cdot}10^{-3}$	$3.2{\cdot}10^{-2}$	0.124	0.251
Diamond					
SANA	$9.1{\cdot}10^{-6}$	$1.4{\cdot}10^{-2}$	$5.5{\cdot}10^{-2}$	0.197	0.429
FEM	$9.5{\cdot}10^{-5}$	$1.4{\cdot}10^{-2}$	$5.5{\cdot}10^{-2}$	0.209	0.422

VI. Conclusion

This paper presents a complete 3D model derivation for accurate modeling of slotless PM machines with different winding shapes, including skewed. This semi-analytical approach does allow to calculate the magnetic field in all regions and electric field in regions with an assigned conductivity. More specifically this paper discussed extraction of the induced rotor eddy-current losses using semi-analytical model. This approach is based on a magnetic field derivation from the Maxwell equations by means of magnetic vector potential and magnetic second order vector potential in the cylindrical coordinates. The source of the armature reaction is implemented using a linear current density which is expressed as Fourier series.

To validate the model, three benchmark slotless PM machines with fixed parameter Faulhaber, rhombic and diamond windings have been modeled. The obtained results

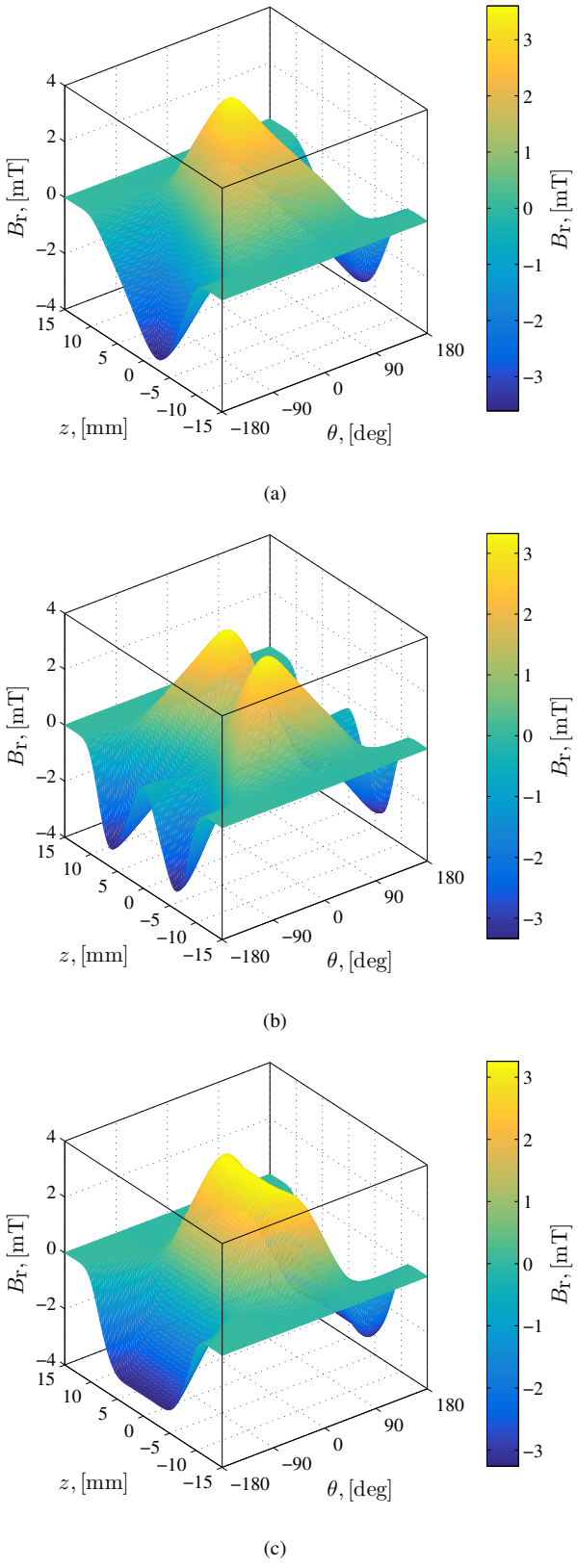

Figure 6: Radial component of the armature reaction magnetic flux density of the benchmark PM machines with a) Faulhaber, b) rhombic, and c) diamond slotless winding types at $r = r_m$.

This article has been accepted for publication in a future issue of this journal, but has not been fully edited. Content may change prior to final publication. Citation information: DOI 10.1109/TMAG.2016.2586740, IEEE Transactions on Magnetics

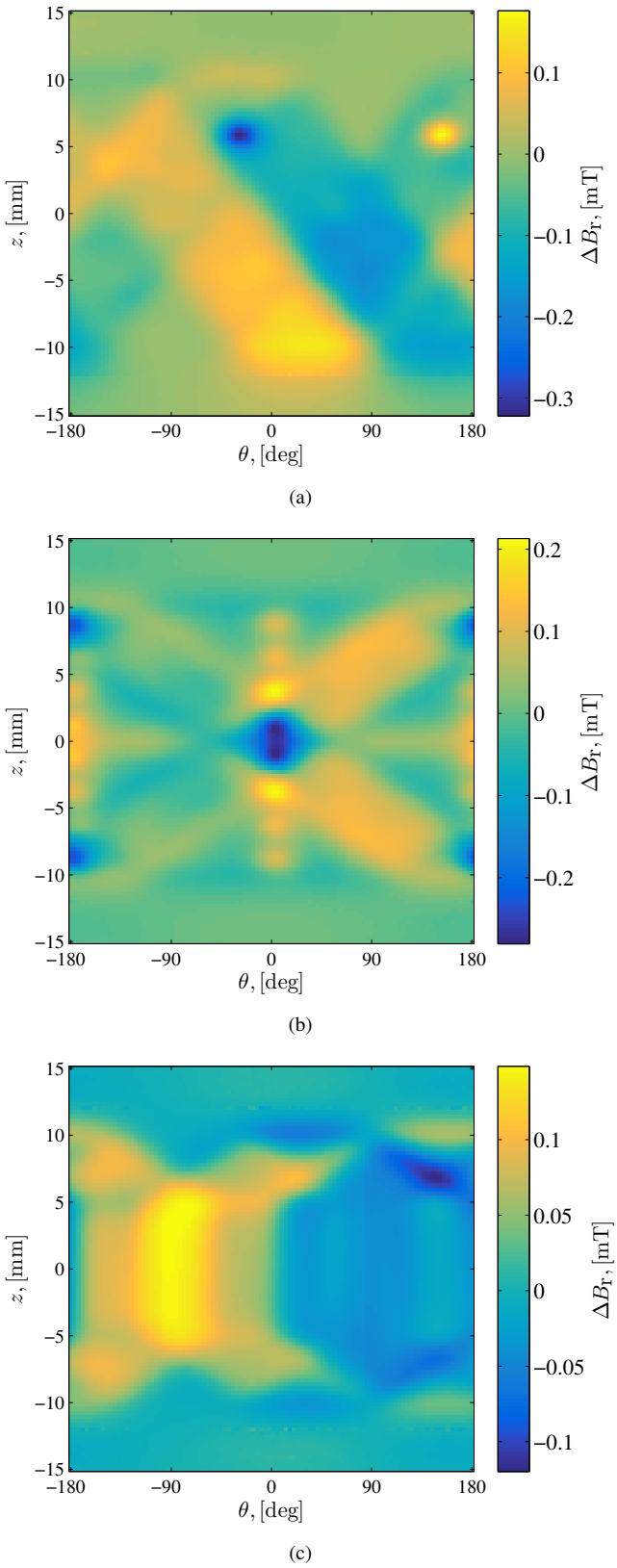

Figure 7: Relative difference between radial component of the armature reaction flux densities obtained semi-analytically and by 3D FEM for the benchmark PM machines with a) Faulhaber, b) rhombic, and c) diamond slotless winding types at $r = r_{\mathrm{m}}$.

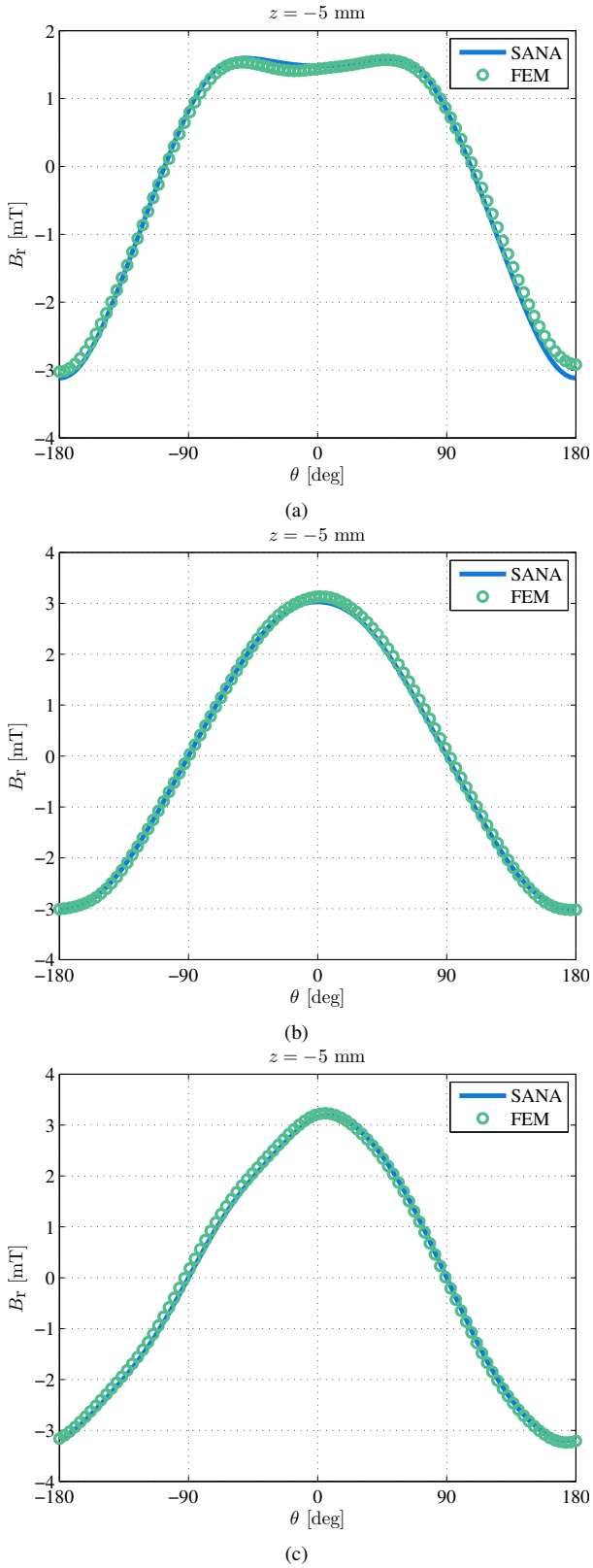

Figure 8: Relative difference between radial component of armature reaction flux densities obtained by a semi-analytically (SANA) and a 3D FEM (FEM) for the benchmark PM machines with a) Faulhaber, b) rhombic, and c) diamond slotless winding types at $r = r_{\mathrm{m}}$ and $z = -5$ mm.

This article has been accepted for publication in a future issue of this journal, but has not been fully edited. Content may change prior to final publication. Citation information: DOI 10.1109/TMAG.2016.2586740, IEEE Transactions on Magnetics

have been compared with those obtained by 3D FEM, and this comparison showed a good agreement. The discrepancy, between magnetic flux density and rotor eddy-current losses, had a maximum of 10% and 5%, respectively, between the 3D semi-analytical and 3D FEM models for the benchmark machines. The calculation time of semi-analytical approach for all winding configurations is less than a minute where for the 3D FEM it takes a few days to reach the steady-state point, assuming equal hardware conditions. For slotless PM machines with comparable winding shapes and physics as the benchmark topologies, 3D harmonic modeling has proven to be an excellent tool for modeling and design optimization in terms of computational time, as well as accuracy.

APPENDIX

A. Linear current density of rhombic winding

To calculate the axial component of the linear current density distribution, the rhombic winding is divided into four current carrying filaments as shown in Fig. 9. Following the coefficients in the distribution function (25) are derived using (26) as

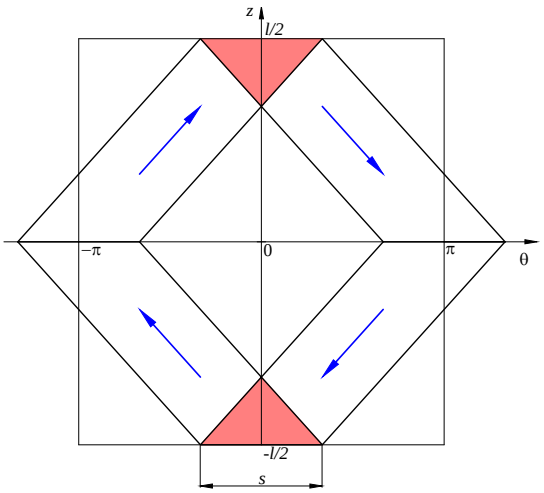

Figure 9: A phase coil of a rhombic winding represented as the four current carrying strips. The blue arrows represent the current direction.

$$c_{\mathrm{ss}} = \frac{\kappa}{4 \cdot 2l \cdot 2\pi} \cdot \left(\int_0^{l/2} \int_{\theta_1}^{\theta_2} \sin\left(\frac{\nu 2\pi}{2\pi}\theta\right) \sin\left(\frac{m2\pi}{2l}z\right) d\theta dz - \int_0^{l/2} \int_{\theta_3}^{\theta_4} \sin\left(\frac{\nu 2\pi}{2\pi}\theta\right) \sin\left(\frac{m2\pi}{2l}z\right) d\theta dz + \int_{-l/2}^{0} \int_{\theta_5}^{\theta_6} \sin\left(\frac{\nu 2\pi}{2\pi}\theta\right) \sin\left(\frac{m2\pi}{2l}z\right) d\theta dz - \int_{-l/2}^{0} \int_{\theta_7}^{\theta_8} \sin\left(\frac{\nu 2\pi}{2\pi}\theta\right) \sin\left(\frac{m2\pi}{2l}z\right) d\theta dz \right), \quad (44)$$

$$c_{\mathrm{sc}} = \frac{\kappa}{4 \cdot 2l \cdot 2\pi} \cdot \left(\int_0^{l/2} \int_{\theta_1}^{\theta_2} \sin\left(\frac{\nu 2\pi}{2\pi}\theta\right) \cos\left(\frac{m2\pi}{2l}z\right) d\theta dz - \int_0^{l/2} \int_{\theta_3}^{\theta_4} \sin\left(\frac{\nu 2\pi}{2\pi}\theta\right) \cos\left(\frac{m2\pi}{2l}z\right) d\theta dz + \int_{-l/2}^{0} \int_{\theta_5}^{\theta_6} \sin\left(\frac{\nu 2\pi}{2\pi}\theta\right) \cos\left(\frac{m2\pi}{2l}z\right) d\theta dz - \int_{-l/2}^{0} \int_{\theta_7}^{\theta_8} \sin\left(\frac{\nu 2\pi}{2\pi}\theta\right) \cos\left(\frac{m2\pi}{2l}z\right) d\theta dz \right), \quad (45)$$

$$c_{\mathrm{cs}} = \frac{\kappa}{4 \cdot 2l \cdot 2\pi} \cdot \left(\int_0^{l/2} \int_{\theta_1}^{\theta_2} \cos\left(\frac{\nu 2\pi}{2\pi}\theta\right) \sin\left(\frac{m2\pi}{2l}z\right) d\theta dz - \int_0^{l/2} \int_{\theta_3}^{\theta_4} \cos\left(\frac{\nu 2\pi}{2\pi}\theta\right) \sin\left(\frac{m2\pi}{2l}z\right) d\theta dz + \int_{-l/2}^{0} \int_{\theta_5}^{\theta_6} \cos\left(\frac{\nu 2\pi}{2\pi}\theta\right) \sin\left(\frac{m2\pi}{2l}z\right) d\theta dz - \int_{-l/2}^{0} \int_{\theta_7}^{\theta_8} \cos\left(\frac{\nu 2\pi}{2\pi}\theta\right) \sin\left(\frac{m2\pi}{2l}z\right) d\theta dz \right), \quad (46)$$

This article has been accepted for publication in a future issue of this journal, but has not been fully edited. Content may change prior to final publication. Citation information: DOI 10.1109/TMAG.2016.2586740, IEEE Transactions on Magnetics

$$c_{\mathrm{cc}} = \frac{\kappa}{4 \cdot 2l \cdot 2\pi} \cdot \cdot \left(\int_0^{l/2} \int_{\theta_1}^{\theta_2} \cos\left(\frac{\nu 2\pi}{2\pi}\theta\right) \cos\left(\frac{m2\pi}{2l}z\right) d\theta dz - \right. - \int_0^{l/2} \int_{\theta_3}^{\theta_4} \cos\left(\frac{\nu 2\pi}{2\pi}\theta\right) \cos\left(\frac{m2\pi}{2l}z\right) d\theta dz + + \int_{-l/2}^{0} \int_{\theta_5}^{\theta_6} \cos\left(\frac{\nu 2\pi}{2\pi}\theta\right) \cos\left(\frac{m2\pi}{2l}z\right) d\theta dz - \left. - \int_{-l/2}^{0} \int_{\theta_7}^{\theta_8} \cos\left(\frac{\nu 2\pi}{2\pi}\theta\right) \cos\left(\frac{m2\pi}{2l}z\right) d\theta dz \right), \quad (47)$$

where

$$\begin{aligned} \theta_1 &= \frac{2\pi z}{l} - \frac{4\pi}{3}, \\ \theta_2 &= \frac{2\pi z}{l} - \frac{2\pi}{3}, \\ \theta_3 &= \frac{2\pi(l/2 - z)}{l} - \frac{\pi}{3}, \\ \theta_4 &= \frac{2\pi(l/2 - z)}{l} + \frac{\pi}{3}, \\ \theta_5 &= -\frac{2\pi z}{l} - \frac{4\pi}{3}, \\ \theta_6 &= -\frac{2\pi z}{l} - \frac{2\pi}{3}, \\ \theta_7 &= \frac{2\pi(l/2 + z)}{l} - \frac{\pi}{3}, \\ \theta_8 &= \frac{2\pi(l/2 + z)}{l} + \frac{\pi}{3}. \end{aligned} \quad (48)$$

These coefficients contain four integrals, which correspond to the number of current carrying filaments, and the sign, preceeding the integrals, shows the directions of current with respect to the axial direction. The limits of the inner integrals are the equations of the filament border lines, where these dependencies can be derived as

$$\theta = (z - z_0)\frac{\theta_1 - \theta_0}{z_1 - z_0} + \theta_0. \quad (49)$$

These coefficients should be calculated for the following cases

$$\begin{aligned} &1^{\mathrm{st}} \text{ case, for } \nu > 0,\ m > 0, \\ &2^{\mathrm{nd}} \text{ case, for } \nu = 0,\ m > 0, \\ &3^{\mathrm{rd}} \text{ case, for } \nu > 0,\ m = 0, \\ &4^{\mathrm{th}} \text{ case, for } \nu = 0,\ m = 0, \end{aligned} \quad (50)$$

which eventually results in nine coefficients. In the case of the rhombic winding, only coefficients c_{ss} and c_{sc} for ($\nu > 0$, $m > 0$) do not result in a zero. Following some mathematical simplifications the distribution function of three phases for the rhombic winding is

$$\begin{aligned} f(\theta, z) = & \\ \sum_{\substack{\nu=1 \\ m=1}}^{\infty} & \left(\frac{c_{\mathrm{ss}} + c_{\mathrm{sc}}}{2} \sin\left(\nu(\theta + x)\right) \cos\left(\frac{\left(n - \frac{m}{2}\right)\pi}{l} z \right) + \right. \\ & \left. + \frac{c_{\mathrm{ss}} - c_{\mathrm{sc}}}{2} \sin\left(\nu(\theta + x)\right) \cos\left(\frac{\left(n + \frac{m}{2}\right)\pi}{l} z \right) \right), \quad (51) \\ c_{\mathrm{ss}} &= \frac{16\cos(n\pi)\sin(m\pi/4)^2\sin(n\pi/3)}{mn\pi^2}, \\ c_{\mathrm{sc}} &= -\frac{8\sin(m\pi/2)\sin(n\pi/3)\sin(n\pi)}{mn\pi^2}, \\ x &= (0, \frac{2\pi}{3}, \frac{4\pi}{3}). \end{aligned}$$

Substituting this distribution function into (24) and having in mind the following trigonometric identity:

$$\sin(\alpha)\cos(\beta) = \frac{\sin(\alpha + \beta) + \sin(\alpha - \beta)}{2}, \quad (52)$$

the axial component of the linear current density for the rhombic winding is

$$\begin{aligned} K_{\mathrm{z}}(\theta, z, t) = & \sum_{\substack{m=1 \\ k=1 \\ L=-\infty}}^{\infty} \\ & \left(\hat{K}_{\mathrm{sc1}}(m,k,L) \sin\left(((3L-k)\theta + k\omega t)\right) \cos(\omega_{\mathrm{z1}} z) + \right. \\ & \left. + \hat{K}_{\mathrm{sc2}}(m,k,L) \sin\left(((3L-k)\theta + k\omega t)\right) \cos(\omega_{\mathrm{z2}} z) \right), \quad (53) \\ \omega_{\mathrm{z1}} &= \frac{\left(3L - k - \frac{m}{2}\right)\pi}{l}, \\ \omega_{\mathrm{z2}} &= \frac{\left(3L - k + \frac{m}{2}\right)\pi}{l}, \\ \hat{K}_{\mathrm{sc1}} &= \\ & \frac{3N\hat{I}}{2sr_{\mathrm{si}}} \frac{16\cos((3L-k)\pi)\sin(m\pi/4)^2\sin((3L-k)\pi/3)}{m(3L-k)\pi^2}, \\ \hat{K}_{\mathrm{sc2}} &= \\ & -\frac{3N\hat{I}}{2sr_{\mathrm{si}}} \frac{8\sin(m\pi/2)\sin((3L-k)\pi/3)\sin((3L-k)\pi)}{m(3L-k)\pi^2}, \end{aligned}$$

B. Linear current density of Faulhaber winding

$$K_{\mathrm{z}}(\theta,z,t)=\sum_{\substack{m=1\\k=1\\L=-\infty}}^{\infty}\hat{K}_{\mathrm{sc}}\sin\left(((3L-k)\theta+k\omega t)\right)\cdot$$
$$\cdot\left(\sin\left(\omega_{\mathrm{z}1}z+\frac{(3L-k)\pi}{2}\right)+\sin\left(\omega_{\mathrm{z}2}z+\frac{(3L-k)\pi}{2}\right)\right)+$$
$$+\sum_{\substack{k=1\\L=-\infty}}^{\infty}\hat{K}_{\mathrm{s}}\sin\left(((3L-k)\theta+k\omega t)\right)\sin\left(\omega_{\mathrm{z}3}z+\frac{(3L-k)\pi}{2}\right), \tag{54}$$
$$\omega_{\mathrm{z}1}=\frac{(3L-k+m)\,\pi}{2l},$$
$$\omega_{\mathrm{z}2}=\frac{(3L-k-m)\,\pi}{2l},$$
$$\omega_{\mathrm{z}3}=\frac{(3L-k)\,\pi}{2l},$$
$$\hat{K}_{\mathrm{sc}}=\frac{3N\hat{I}}{2sr_{\mathrm{si}}}\frac{4\sin(m\pi/2)\sin((3L-k)\pi/3)}{m(3L-k)\pi^2},$$
$$\hat{K}_{\mathrm{s}}=\frac{3N\hat{I}}{2sr_{\mathrm{si}}}\frac{2\sin((3L-k)\pi/3)}{(3L-k)\pi}.$$

C. Linear current density of diamond winding

$$K_{\mathrm{z}}(\theta,z,t)=\sum_{\substack{m=1\\k=1\\L=-\infty}}^{\infty}$$
$$\left(\hat{K}_{\mathrm{ss}}\sin\left(((3L-k)\theta+k\omega t)\right)\left(\cos(\omega_{\mathrm{z}1}z)+\cos(\omega_{\mathrm{z}2}z)\right)+\right.$$
$$\left.+\hat{K}_{\mathrm{sc}}\sin\left(((3L-k)\theta+k\omega t)\right)\cos\left(\frac{m\pi}{2l}z\right)\right)+$$
$$+\sum_{\substack{k=1\\L=-\infty}}^{\infty}\hat{K}_{\mathrm{s}}\sin\left(((3L-k)\theta+k\omega t)\right), \tag{55}$$
$$\omega_{\mathrm{z}1}=\frac{\left(3L-k-\frac{m}{2}\right)\pi}{l},$$
$$\omega_{\mathrm{z}2}=\frac{\left(3L-k+\frac{m}{2}\right)\pi}{l},$$
$$\hat{K}_{\mathrm{ss}}=\frac{3N\hat{I}}{2sr_{\mathrm{si}}}\frac{16(1+2\cos(m\pi/4))\cos((3L-k)\pi)}{2m(3L-k)\pi^2}\cdot$$
$$\cdot\sin(m\pi/8)^2\sin(\pi(3L-k)/3),$$
$$\hat{K}_{\mathrm{sc}}=$$
$$-\frac{3N\hat{I}}{2sr_{\mathrm{si}}}\frac{8\sin(m\pi/4)\sin((3L-k)\pi/3)\sin((3L-k)\pi/2)}{m(3L-k)\pi^2},$$

$$\hat{K}_{\mathrm{s}}=-\frac{3N\hat{I}}{2sr_{\mathrm{si}}}\frac{2(2\cos((3L-k)\pi/6)+\cos((3L-k)\pi/2))}{(3L-k)\pi}\cdot$$
$$\cdot\sin((3L-k)\pi/6)^2.$$

REFERENCES

[1] B. L. J. Gysen, K. J. Meessen, J. J. H. Paulides, and E. A. Lomonova, "General formulation of the electromagnetic field distribution in machines and devices using fourier analysis," *Magnetics, IEEE Transactions on*, vol. 46, pp. 39–52, Jan 2010.

[2] A. Borisavljevic, *Limits, Modeling and Design of High-Speed Permanent Magnet Machines*. Springer-Verlag Berlin Heidelberg, 2013.

[3] P.-D. Pfister and Y. Perriard, "Slotless permanent-magnet machines: General analytical magnetic field calculation," *Magnetics, IEEE Transactions on*, vol. 47, pp. 1739–1752, June 2011.

[4] S. Holm, *Modeling and optimization of a permanent magnet machine in a flywheel*. PhD thesis, Delft University of Technology, 2003.

[5] P. Ragot, M. Markovic, and Y. Perriard, "Analytical determination of the phase inductances for a brushless dc motor with faulhaber windings," *Industry Applications, IEEE Transactions on*, vol. 45, pp. 1360–1366, 2010.

[6] E. Matagne, B. Dehez, and K. Ben-Naoum, "Exact special 2d spectral expression of the magnetic field in air gap with skewed source," in *Electrical Machines (ICEM), 2012 XXth International Conference on*, pp. 2825–2831, Sept 2012.

[7] A. Anderson, J. Bumby, and B. Hassall, "Analysis of helical armature windings with particular reference to superconducting a.c. generators," *Generation, Transmission and Distribution, IEE Proceedings C*, vol. 127, no. 3, pp. 129–144, 1980.

[8] S. Jumayev, J. J. H. Paulides, K. O. Boynov, J. Pyrhonen, and E. A. Lomonova, "Three-dimensional analytical model of helical winding pm machines including rotor eddy-currents," *Magnetics, IEEE Transactions on*, vol. PP, no. 99, pp. 1–1, 2016.

[9] K. Weigelt, *Über die dreidimensionale analytische Berechnung von Wirbelströmen in gekoppelten Kreiszylinderschalen*. PhD thesis, Technischen Universität München, 1986.

[10] B. Hague, *The Principles of Electromagnetism Applied to Electrical Machines*. Dover Publications, inc., 1962.

[11] W. R. Smythe, *Static and dynamic electricity*. New York : McGraw-Hill, 3rd ed ed., 1967. Includes bibliographies.

[12] P. Hammond, "Use of potentials in calculation of electromagnetic fields," *Physical Science, Measurement and Instrumentation, Management and Education - Reviews, IEE Proceedings A*, vol. 129, pp. 106–112, March 1982.

[13] T. Theodoulidis, C. S. Antonopoulos, and E. E. Kriezis, "Analytical solution for the eddy current problem inside a conducting cylinder using the second order magnetic vector potential," *COMPEL - The International Journal for Computation and Mathematics in Electrical and Electronic Engineering*, vol. Vol. 14, No. 4, pp. 45–48, 1995.

[14] K. J. W. Pluk, J. W. Jansen, and E. A. Lomonova, "Modeling of noncuboidal magnetic sources in 3-d fourier modeling," *Magnetics, IEEE Transactions on*, vol. 51, pp. 1–4, Nov 2015.